JOURNAL OF SYNCHROTRON RADIATION

ISSN 1600-5775

Time-resolved *in situ* tomography for the analysis of evolving metal-foam granulates

Francisco García-Moreno,[a,b]* Paul H. Kamm,[a] Tillmann R. Neu[a] and John Banhart[a,b]

[a]Helmholtz-Zentrum Berlin für Materialien und Energie, Hahn-Meitner-Platz 1, Berlin 14109, Germany, and [b]Technische Universität Berlin, Hardenbergstrasse 36, Berlin 10623, Germany.
*Correspondence e-mail: garcia-moreno@helmholtz-berlin.de

Received 21 March 2018
Accepted 19 June 2018

Edited by M. Yabashi, RIKEN SPring-8 Center, Japan

Keywords: time-resolved tomography; *in situ* tomography; dynamic processes; metal-foam granulates.

Supporting information: this article has supporting information at journals.iucr.org/s

An experimental setup has been developed that allows for capturing up to 25 tomograms s^{-1} using the white X-ray beam at the experimental station EDDI of BESSY II, Berlin, Germany. The key points are the use of a newly developed, precise and fast rotation stage, a very efficient scintillator and a fast CMOS camera. As a first application, the foaming of aluminium alloy granules at 923 K was investigated *in situ*. Formation and growth of bubbles in the liquid material were observed and found to be influenced by the limited thermal conductivity in the bulk granules. Changes that took place between two tomographic frames separated in time by 39 ms could be detected and analysed quantitatively.

1. Introduction

Dynamic processes in evolving metallic foams have been studied *in situ* using fast X-ray radioscopy (Garcia-Moreno *et al.*, 2008, 2012; Rack *et al.*, 2009). Although acquisition rates over 100000 frames s^{-1} have been reached (Garcia-Moreno *et al.*, 2012), and valuable insights into the dynamics of foaming and the corresponding morphological changes in foams have been gained, radiographic information is often ambiguous and limited to flat sample configurations. *In situ* tomography lifts some of the restrictions but is too slow for real-time studies.

Recent developments have led to higher temporal resolutions through improved instrument hardware and data processing capabilities. Acquisition times are also becoming shorter because of the use of high-brilliance third-generation synchrotron sources, highly efficient scintillators and improved optics. As a consequence, fast tomography with up to 20 tomograms s^{-1} (20 Hz) has become available at different beamlines (Rack *et al.*, 2010; Momose *et al.*, 2011; Takano *et al.*, 2013; Mokso *et al.*, 2015; Maire *et al.*, 2016; Kamm *et al.*, 2017; dos Santos Rolo *et al.*, 2014; Lovric *et al.*, 2016). Evolving metallic foams (García-Moreno *et al.*, 2013; Jiménez *et al.*, 2018; Kamm *et al.*, 2017) can now be studied in real time with *in situ* tomography. Furthermore, *operando* studies such as cycling of rechargeable batteries (Schröder *et al.*, 2016) or operating fuel cells (Alrwashdeh *et al.*, 2017) are currently the focus of research.

In this work, we present the latest development in imaging acquisition speed at the EDDI beamline at BESSY II, Berlin, Germany, where we are now able to perform time-resolved *in situ* tomography up to 25 Hz, which is the fastest tomography acquisition rate reported at synchrotrons so far. As a case study, we analyse the foaming behaviour of a metallic foam granulate. Similar to polymeric foams, the use of

© 2018 International Union of Crystallography

expandable granulates is interesting from an application point of view. As the surface-to-volume ratio of granules compared with standard bulk precursors is much larger, their foaming behaviour might suffer from insufficient gas nucleation or increased gas losses, incomplete particle bonding, and result in non-uniform pore sizes and foam densities (Duarte *et al.*, 2013; Nosko *et al.*, 2010). Therefore we study the foaming behaviour of single granulates and the evolution of the time-resolved bubble size.

2. Experimental procedure

A new high-speed rotation stage (see Fig. 1) jointly developed at the Helmholtz–Zentrum, Berlin, and the Technische Universität Berlin is used. Here, we explore fast phenomena in evolving metal foams with a rotation frequency of ∼12.5 Hz, which allows us to capture tomograms at ∼25 Hz, each of which requires a rotation by 180°. The stage features a precision rotation axis with ball bearings and a servo drive regulated by an angular PID speed controller with sensor feedback from the servo drive, programmable by self-developed *Labview*-based software. No electric sliding contacts for the rotation system are available, which is why heating and temperature measurements are conducted contactless. Special attention has been paid to centering samples and crucibles precisely as no *xy* table was used, and centrifugal forces reach 0.6*g* at the inner side of the crucible of radius $r_i \simeq 1$ mm.

AlSi10 + 0.5 TiH_2 (all in wt%) foamable precursor granulate (equivalent diameter $\simeq$ 1 mm) is produced following the powder metallurgical route described elsewhere (Banhart, 2006). The granules are placed in an X-ray-transparent boron nitride (BN) crucible of 2.2 mm inner and 3 mm outer diameter. Foaming is induced by heating the samples in the crucible with a ramp of ∼2 K s^{-1} to around 923 K using a 150 W IR lamp (Osram, Germany) from the top (see Fig. 1). Foaming starts during the heating phase at around 853 K, close to the eutectic temperature of the Al–Si alloy (850 K) when the system is not under isothermal conditions.

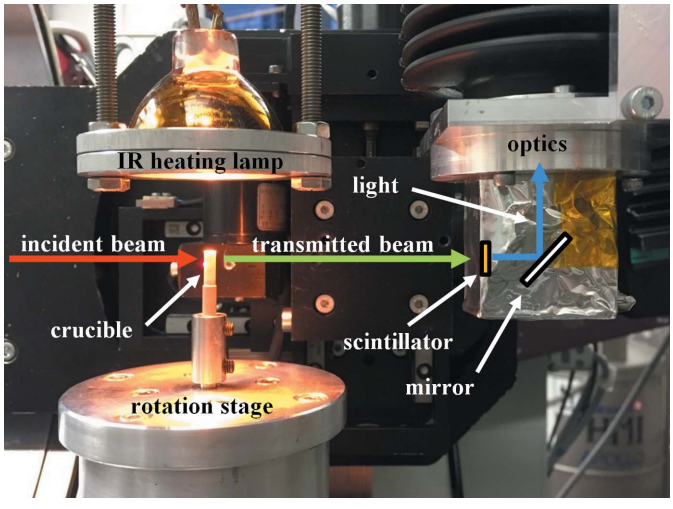

Figure 1
Time-resolved *in situ* tomography setup installed at the EDDI instrument, composed of a fast rotation stage, an IR heating lamp (for temperatures up to 1073 K), an X-ray transparent BN crucible, a 200 µm-thick LuAG:Ce scintillator, a white-beam optical system configuration and a PCO Dimax CMOS camera. The incident (red) and transmitted (green) X-ray beams as well as the light path from the scintillator to the camera (blue) are shown.

A white X-ray beam (about 6–120 keV) is provided by a superconducting 7 T multipole wiggler. A 200 µm-thick LuAG:Ce scintillator is used to convert the transmitted images into visible light, after which a mirror projects the light onto a PCO Dimax CMOS camera. A more detailed explanation of the imaging system can be found elsewhere (Jiménez *et al.*, 2018; García-Moreno *et al.*, 2013).

A compromise between pixel size, field of view (FOV), number of projections and rotation speed is necessary depending on the experiment type and requirements. In the present case, the acquisition parameters are: a spatial resolution of 5 µm measured on a micro-resolution test pattern from JIMA, Japan, an FOV of 3.44 mm × 1.85 mm (given by the pixel size of 2.5 µm), an exposure time of 0.48 ms for each single projection, 78 projections per tomogram (sufficient for our purpose), and a time resolution of ∼39 ms per tomogram. The Common Unified Device Architecture (CUDA)-accelerated filtered back-projection (FBP) algorithm-based reconstruction is performed using the open source *ASTRA Toolbox* (van Aarle *et al.*, 2016). Tomograms at 25.6 Hz are acquired in 15.5 s.

3. Results and discussion

A total of 396 tomograms were acquired in ∼15.5 s in order to follow the stage of gas nucleation and subsequent bubble evolution in AlSi10 + 0.5 TiH_2 granules as they were heated. The high rate of ∼25 Hz allows us to resolve, *in situ* and in detail, the bubble evolution inside each single granule. Fig. 2(*c*) shows six *xy*-slices at a particular height (z = 1.4 mm) extracted from the series of 396 tomograms. Nucleation probably starts around $t \simeq 0$ s in the granule (see lower right image), but in fact we only observe bubble growth in the early stages because nucleation itself is not observable due to insufficient spatial resolution. Pores of 1–2 µm diameter contribute most to the total bubble volume in the nucleation stage of Zn foams as measured by neutron scattering but pores as small as 50 nm could also be detected (Banhart *et al.*, 2001). We assume that each appearing bubble corresponds to a single nucleus (Kamm *et al.*, 2017). At $t \simeq 2.5$ s and 5 s, the second (lower left) and third (middle) granules follow as manifested by the appearance of the first bubbles, respectively. The different onset times are understandable because the heat applied is transmitted into the grains from the direction of the heating lamp and through the crucible walls, and there is a small radial and a larger axial temperature gradient inside the crucible. Moreover, intergranular heat transfer is low because of the small contact area between granules, which leads to a slight temperature delay in some particles depending on their location. This observation underlines a difference to bulk samples and can explain the varying pore sizes and densities of solidified foams made from granules reported in the literature

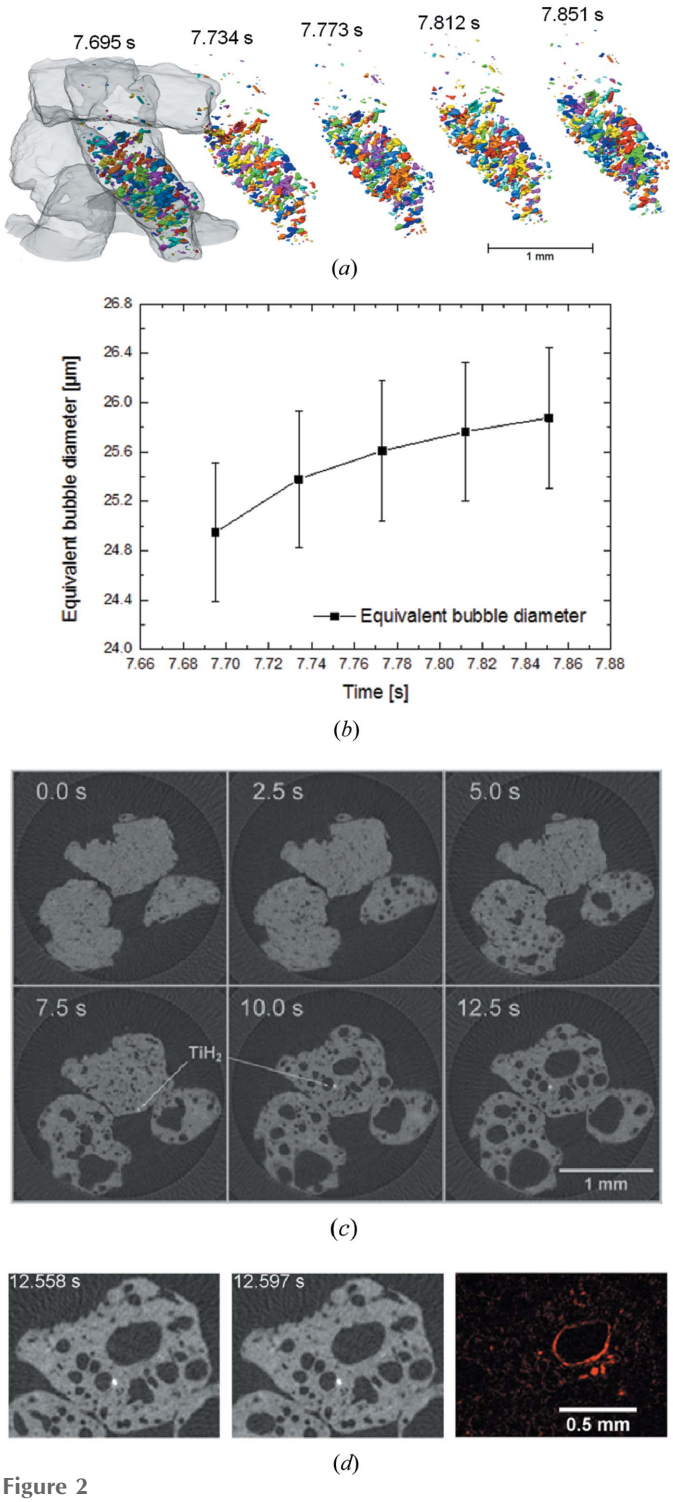

Figure 2
Time-resolved tomography (∼25 Hz) of AlSi10 + 0.5 wt% TiH_2 precursor granules foaming at ∼923 K in a cylindrical BN crucible. (*a*) Tomogram of several granules at t = 7.695 s, with bubbles coloured for the central granule, and time evolution of the bubbles in this granule over five tomograms, each separated by only 39 ms. (*b*) Time evolution of the mean-equivalent bubble diameter over 156 ms corresponding to (*a*). (*c*) Series of six two-dimensional slices, each separated by 2.5 s, as extracted from the series recorded over 15.5 s during foaming, and showing the appearance and growth of gas bubbles and foam evolution. Small white dots correspond to TiH_2 particles. (*d*) Two two-dimensional slices of one granule at t = 12.558 s and t = 12.597 s and the corresponding difference image showing changes in red.

(Nosko *et al.*, 2010). On the other hand, intragranular nucleation takes place almost simultaneously as a result of good heat transfer within individual granules similar to bulk samples (Kamm *et al.*, 2017).

The tomogram at t = 7.695 s shown in Fig. 2(*a*) as a three-dimensional rendering features several granules in transparent grey and a selected grain with individual bubbles internally highlighted by different colours, obtained by binarization and segmentation of the image. It also shows the same single granule again four more times within time intervals of 39 ms (*i.e.* at t = 7.734 s, 7.773 s, 7.812 s and 7.851 s), thus exploiting the maximal temporal resolution of our experiment. This visual comparison together with the corresponding analysis of the mean equivalent diameter of all bubbles (Fig. 2*b*) reveals the changes in bubble size and distribution within these very small time intervals. This result underlines the highly dynamic nature of foaming, although the difference in this short period is smaller than the standard error of the mean diameters. The number of bubbles remains nearly constant at 1298 ± 24, between t = 7.695 s and t = 7.851 s, suggesting that already at this early foaming stage there is no more nucleation or that there is a balance between newly appearing bubbles and those that already start to merge or disappear. The foam bubble evolution at a later stage (t = 12.558 s and t = 12.597 s) is depicted in Fig. 2(*d*), where the difference image shows in red the changes between the two slices (*e.g.* shrinkage of the central bubble and rupture of a smaller one), thus emphasizing the need of such high spatio-temporal resolution.

4. Conclusions

Time-resolved tomography up to 25.6 Hz is now available as a powerful characterization tool for *in situ* analyses in material science.

Granules of AlSi10 alloy + TiH_2 of ∼1 mm equivalent diameter have been foamed and their foaming sequence is found to be dependent on their position. This can be explained by an inferior intergranular thermal contact, although intragranular bubble size evolution is found to be comparable with that of bulk precursors.

The distribution of equivalent bubble-size diameters and their mean values evolve even within the short time between two tomograms (39 ms), thus emphasizing the need for high temporal resolution.

Funding information

Funding by the European Space Agency (project AO-99-075) and German Research Foundation (project BA 1170/35-1 and GA 1304/5-1) is gratefully acknowledged.

References

Aarle, W. van, Palenstijn, W. J., Cant, J., Janssens, E., Bleichrodt, F., Dabravolski, A., De Beenhouwer, J., Joost Batenburg, K. & Sijbers, J. (2016). *Opt. Express*, **24**, 25129–25147.

Alrwashdeh, S. S., Manke, I., Markötter, H., Haußmann, J., Arlt, T., Hilger, A., Al-Falahat, A. M., Klages, M., Scholta, J. & Banhart, J. (2017). *Energ. Technol.* **5**, 1612–1618.
Banhart, J. (2006). *Adv. Eng. Mater.* **8**, 781–794.
Banhart, J., Bellmann, D. & Clemens, H. (2001). *Acta Mater.* **49**, 3409–3420.
Duarte, I., Oliveira, M., Garcia-Moreno, F., Mukherjee, M. & Banhart, J. (2013). *Colloids Surf. A Physicochem. Eng. Asp.* **438**, 47–55.
García-Moreno, F., Jiménez, C., Kamm, P. H., Klaus, M., Wagener, G., Banhart, J. & Genzel, C. (2013). *J. Synchrotron Rad.* **20**, 809–810.
Garcia-Moreno, F., Mukherjee, M., Jiménez, C., Rack, A. & Banhart, J. (2012). *Metals*, **2**, 10–21.
Garcia-Moreno, F., Rack, A., Helfen, L., Baumbach, T., Zabler, S., Babcsan, N., Banhart, J., Martin, T., Ponchut, C. & Di Michiel, M. (2008). *Appl. Phys. Lett.* **92**, 3.
Jiménez, C., Kamm, P. H., Plaepow, M., Neu, T., Klaus, M., Wagner, G., Banhart, J., Genzel, C. & García-Moreno, F. (2018). *J. Synchrotron Rad.* Accepted.
Kamm, P. H., García-Moreno, F., Neu, T. R., Heim, K., Mokso, R. & Banhart, J. (2017). *Adv. Eng. Mater.* **19**, 1600550.
Lovric, G., Mokso, R., Schlepütz, C. M. & Stampanoni, M. (2016). *Phys. Med.* **32**, 1771–1778.
Maire, E., Le Bourlot, C., Adrien, J., Mortensen, A. & Mokso, R. (2016). *Int. J. Fract.* **200**, 3–12.
Mokso, R., Schwyn, D. A., Walker, S. M., Doube, M., Wicklein, M., Müller, T., Stampanoni, M., Taylor, G. K. & Krapp, H. G. (2015). *Sci. Rep.* **5**, 8727.
Momose, A., Yashiro, W., Harasse, S. & Kuwabara, H. (2011). *Opt. Express*, **19**, 8423–8432.
Nosko, M., Simančík, F. & Florek, R. (2010). *Mater. Sci. Eng. A*, **527**, 5900–5908.
Rack, A., García-Moreno, F., Baumbach, T. & Banhart, J. (2009). *J. Synchrotron Rad.* **16**, 432–434.
Rack, A., Garcia-Moreno, F., Schmitt, C., Betz, O., Cecilia, A., Ershov, A., Rack, T., Banhart, J. & Zabler, S. (2010). *J. Xray Sci. Technol.* **18**, 429–441.
Santos Rolo, T. dos, Ershov, A., van de Kamp, T. & Baumbach, T. (2014). *Proc. Natl Acad. Sci.* **111**, 3921–3926.
Schröder, D., Bender, C., Arlt, T., Osenberg, M., Hilger, A., Risse, S., Ballauff, M., Manke, I. & Janek, J. (2016). *J. Phys. D Appl. Phys.* **49**, 404001.
Takano, H., Morikawa, M., Konishi, S., Azuma, H., Shimomura, S., Tsusaka, Y., Nakano, S., Kosaka, N., Yamamoto, K. & Kagoshima, Y. (2013). *J. Phys. Conf. Ser.* **463**, 012025.